2014-01-1368

On the Nature of Particulate Emissions from DISI Engines at Cold-Fast-Idle

Author, co-author (Do NOT enter this information. It will be pulled from participant tab in MyTechZone)

Affiliation (Do NOT enter this information. It will be pulled from participant tab in MyTechZone)

Abstract

Particulate emissions from a production gasoline direct injection spark ignition engine were studied under a typical cold-fast-idle condition (1200 rpm, 2 bar NIMEP). The particle number (PN) density in the 22 to 365 nm range was measured as a function of the injection timing with single pulse injection and with split injection. Very low PN emissions were observed when injection took place in the mid intake stroke because of the fast fuel evaporation and mixing processes which were facilitated by the high turbulent kinetic energy created by the intake charge motion. Under these conditions, substantial liquid fuel film formation on the combustion chamber surfaces was avoided. PN emissions increased when injection took place in the compression stroke, and increased substantially when the fuel spray hit the piston. A conceptual model was established for the particulate matter (PM) formation process in which PM is formed by pyrolysis after the normal premixed flame passage in fuel rich plumes originating from liquid films on the cylinder walls. The pyrolysis process is supported by heat conducted from the hot burned gases outside the plume and by the energy released by the pyrolysis reactions. Thus, the "pool fire" often observed is not a diffusion flame since the small amount of residual oxygen in the burned gases cannot support such a flame. The luminosity is radiation from the hot soot particles which are not oxidized after being formed in the pyrolysis reactions. This model was supported by the PN data obtained from sweeping the charge equivalence ratio from lean to rich.

Introduction

Direct injection (DI) is an attractive option for spark ignition (SI) engines. The in-flight fuel evaporation cools the charge, thereby improving the volumetric efficiency and extending the knock margin. These attributes have made the technology an enabler for highly boosted, downsized engines which offer substantial gains in fuel economy [1-4].

An important issue for DISI engines is the particulate matter emissions [5-8]. Particulate number (PN) emissions for small particles are especially of concern, as stringent limits have been established [9]. PN emissions during cold start in DISI engines are substantially higher than those in port-fuel-injection (PFI) engines [5]. For the latter, when the intake valve opens at part-load, the back flow from the cylinder to the intake manifold blows the liquid fuel in the port back into the intake runner, thereby suppressing liquid fuel film formation in the combustion chamber [10]. In DISI engines, however, the in-cylinder fuel jet directly deposits liquid fuel on the cylinder walls. The fuel vapor that emerges from the fuel films produces fuel rich regions which are responsible for PM formation. Visible soot particle radiation, often referred to as "pool fires", has been observed [11-13].

The goals of this paper are:

1. To connect the PN emissions from a production DISI engine to the geometry of the injection process; and
2. To establish a conceptual model describing the process through which particulates form from the vapor emerging from wall fuel films.

Experimental set up

Engine

The experiments were carried out in a production DISI engine (the GM LNF engine). The engine specifications are detailed in Table 1. The engine has cam phasers for both the intake and exhaust valves; the valve timings were fixed at the values given in Table 1. There was essentially no valve-overlap. The spark and injection timings will be specified in the descriptions of the different experiments that were performed.

Table 1.Engine specifications for the GM 2L LNF DISI engine.

Engine type	Inline 4 cylinder
Displacement [cc]	1998
Bore [mm]	86
Stroke [mm]	86
Compression ratio	9.2:1
Fuel system	Side-mounted direct injection
Valve configuration	16 valve DOHC,
Intake valve open/close (0.25 mm lift)	1° / 231° (atdc-intake)

Exhaust valve /open close (0.25 mm lift)	-222 / 0° (atdc-intake)
Max lift (both intake and exhaust)	10.3 mm

The injection geometry is shown in Fig. 1. There is a cup in the piston to allow wall-guided injection. The fuel injector is located between the two intake valves. The valves do not materially interfere with the spray since there is no substantial change in the engine behavior (in terms of PN and HC emissions) when the start-of-injection (SOI) timing is varied over the lift profile.

The fuel used in these experiments was Haltermann HF0 437 calibration gasoline with RON = 96.6 and RVP = 0.61 bar (9 psi). The fuel was supplied by a pressurized cylinder at 5 MPa. The fuel temperature was regulated by a single pass counterflow shell-in-tube heat exchanger and was maintained at a temperature of 20°C.

The engine coolant temperature (ECT) was regulated by a chiller/ heater system. The nominal operating temperature was 20°C. Experiments at ECT = 80$^°$C were also conducted to assess the sensitivity of the results to ECT.

Data were obtained at 1200 rpm and a net indicated mean effective pressure (NIMEP) of 2 bar. This condition is typical of cold-fast-idle in the startup process leading to catalyst light off. Because the operation is at steady state, repeatability and data quality are much better than data obtained during the cranking and speed flare processes. The liner temperature is close to the ECT. The piston temperature is estimated to be 120°C for ECT at 20° C using the simulation results from reference [14]. It should, however be noted that while the piston temperature has reached equilibrium of about 120C in these experiments, in actual cold start, it takes hundreds of seconds for the piston temperature to get to steady state. So the piston temperature in the fast idle period in an actual cold start would be significantly lower.

The air equivalence ratio (λ) is set at stoichiometric for cylinder #4, which is the cylinder from which all measurements were made. This λ value was obtained by carbon balance from the CO_2/CO measurements in the exhaust runner of cylinder #4. The engine was operated with the same injection pulse width to all four cylinders. There was a substantial cylinder-to-cylinder λ variation (up to 10%) because of differences in volumetric efficiency such that when λ for cylinder #4 was stoichiometric, the overall λ, as measured by the exhaust UEGO sensor was lean.

Measurements

In-cylinder pressure was measured by a Kistler 6125 pressure transducer with a flame arrestor. Exhaust CO_2/CO was measured in the exhaust runner of cylinder #4 by an NDIR detector (Horiba MEXA 584L).

PN Measurements

Particle size distributions were measured by a scanning mobility particle sizer (TSI 3934 SMPS). The flow into this analyzer first went through an impactor to remove particles larger than 365nm in diameter. A radioactive source was then used to impart a known electrical charge on the aerosol sample. The particles were then sorted by a mobility classifier and counted by a condensation particle counter. The measurement range was from 9.3 to 365 nm. In the results to be presented, the total particle number (PN) refers to the integral of the particle size distribution from 22 to 365 nm.

To prevent particle agglomeration in the sample and instrument saturation, the sample was diluted by a stream of nitrogen. The dilution ratio was measured by the CO2 concentration measurements at the exhaust port sampling point by a Horiba MEXA 584L CO_2 meter, and at the SMPS inlet by a more sensitive Licor LI-820 CO_2 analyzer. The typical dilution ratio was approximately 100:1. All of the values reported in this paper have been corrected for dilution.

The exhaust sampling point was at 10 cm from the exhaust valve of cylinder #4. There are significant pressure pulsations at this location. To maintain a steady sampling flow to the dilution system, a heated "T" design similar to that used in the fast-response HC analyzer [15] was used (see Fig. 2). The exhaust gas flow rate is limited by orifice tube 1. The flow through this orifice tube pulsates corresponding to the exhaust pressure. At the inlet of orifice tube 2, however, the pressure is essentially constant at atmospheric; thus, with the dilution tunnel under a slight vacuum, a constant sample flow rate into the dilution system could be maintained. Both orifice tubes have an ID of 0.5 mm and length of 5 cm.

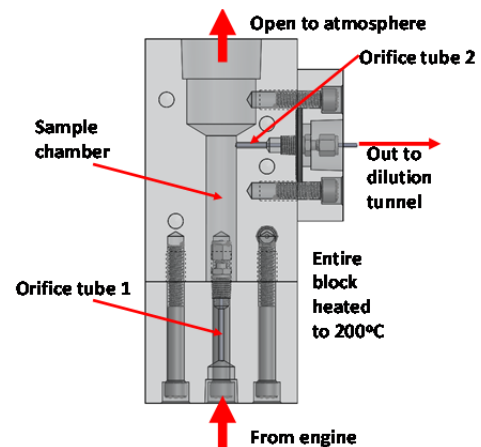To minimize condensation and particle loss through thermophoresis, the entire system was heated to 200° C.

Figure 2. Arrangement to isolate exhaust pressure pulsations in order to achieve a constant sample flow to the sample dilution system.

Results

Single injection

The PN emissions (integration of the size spectrum from 22-365 nm) were measured at the exhaust runner of cylinder #4 as a function of start of injection (SOI) timing at a fast idle condition (1200 rpm, 2 bar NIMEP) with ECT = 20°C. The injection duration varied from 0.76 to 1.05 ms (5.5 to 7.6° crank angle); the fuel mass varied from 9.2 to 12.3 mg per cylinder per cycle, with the latter value being injected late (330° atdc-intake) in the compression stroke. The exhaust λ from a carbon balance was stoichiometric. Since NIMEP and exhaust λ were kept constant, the change in the amount of fuel supplied reflects the amount of fuel not oxidized and, to a lesser extent, the change in thermal efficiency due to changes in combustion phasing. The unconsumed fuel could go into the lubrication system or exit with the exhaust gas as hydrocarbons.

The PN emissions map as a function of SOI and spark timing is shown in Fig. 3. For injections early in the intake stroke, emissions were high; they intensified with spark retard. Emissions decreased with advanced SOI and attained a very low level when the SOI was in the mid compression stroke. The data at a spark timing of -25° atdc-compression are representative of the general trends and are used for further discussion. (Note that normal cold idle runs at much more retarded spark timing (10 to 20° atdc) to obtain a hot exhaust which facilitates catalyst warm up. However, with retarded spark, the engine becomes unstable at later SOI. The early spark timing has been chosen so that a larger SOI sweep data set could be obtained.)
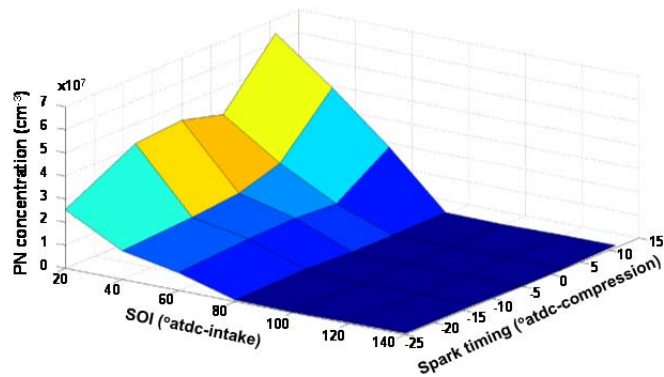

Figure 3. Cold-fast-idle PN emissions as a function of SOI and spark timing; ECT = 20° C.

The PN emissions at -25° atdc-compression spark as a function of SOI are shown in Fig. 4 together with the injection geometry at selected points. The range of SOI timings has been expanded to 330° atdc-intake. Further SOI retard was not attempted because the spark timing is at 335° atdc-intake.
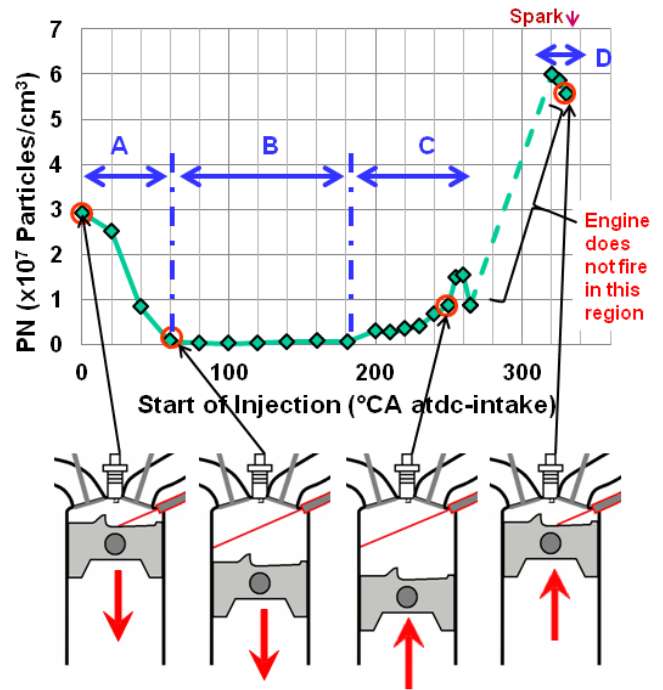

Figure 4. PN as a function of SOI and injection geometry at selected points. Cold-fast-idle at ECT=20° C.

The piston positions in Fig. 4 are drawn at the end of injection. The arrival of the spray at the walls (piston and liner) depends on the spray penetration speed and piston positions at the various SOI timings. CFD results (that finite amount of fuel has landed on the walls) indicate that the spray has reached the walls at the end of injection.

The corresponding COV of NIMEP values are shown in Fig.5. The values were low for SOI in the intake stroke, but increased drastically at SOI timings later than 230° atdc-intake. The engine did not fire with the SOI retarded further than 265° atdc-intake. However, combustion stabilized again when the SOI was retarded to 320° atdc-intake.
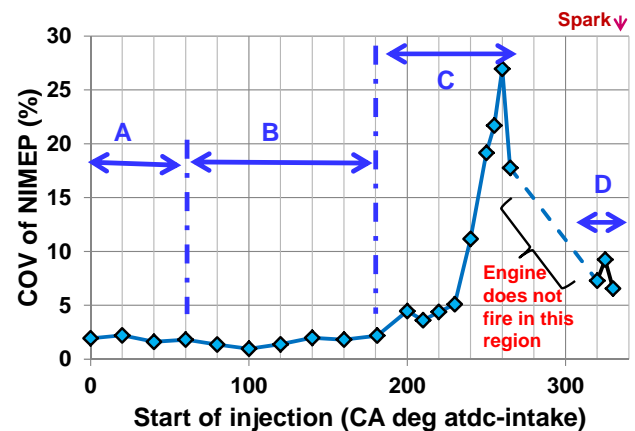

Figure 5. COV of NIMEP corresponding to the data in Fig. 4.

The PN data may be grouped into 4 sets, which are labeled from A to D in Fig. 4 and 5. The behavior of the PN emissions in each set is discussed below.

In set B, the injection was in the mid to late intake stroke. Most of the fuel spray travels the full distance of the combustion chamber before impinging on the walls. Because of the longer time of flight to the surfaces, the wall film mass was lower. See Table 2 for the mass fractions of the fuel that landed on the walls obtained from CFD simulations of selected operating points. The evaporation and mixing processes are facilitated by:

- The large footprint of the impingement area;
- The long duration available for evaporation and mixing prior to combustion; and
- Most significantly, by the highly turbulent charge motion produced by the induction flow (see Fig. 6).

In set B, the evaporation of wall films was largely complete and a well-mixed mixture was formed; see Fig. 7. As a result, for these data, combustion was stable and PN emissions were low. (It should be pointed out that results in Fig. 7 have been obtained at ECT=90° C, which is higher than that (at 20° C) of the experiments. Therefore, the evaporation rate on liner surfaces would be slower. The mixing rates are representative of the experiments.)

Table 2. Fuel mass that landed on combustion chamber walls as a fraction of the injected fuel mass for selected points in Fig. 4 (from a CFD simulation).

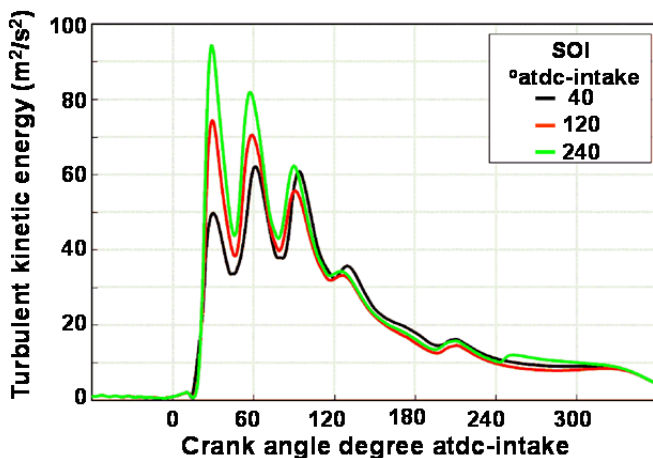| Set	SOI (^{o} CA atdc-intake)	Mass on liner/ mass injected	Mass on piston/ mass injected	total mass landed on walls/ mass injected
A	40	0.6%	20.3%	20.9%
B	120	3.3%	2.4%	5.7%
C	240	9.4%	3.7%	13.1%

Figure 6. Turbulent kinetic energy of the charge. The small differences between the cases are due to the fact that the engine operates at constant NIMEP; so the intake boundary conditions changed as the SOI was varied.
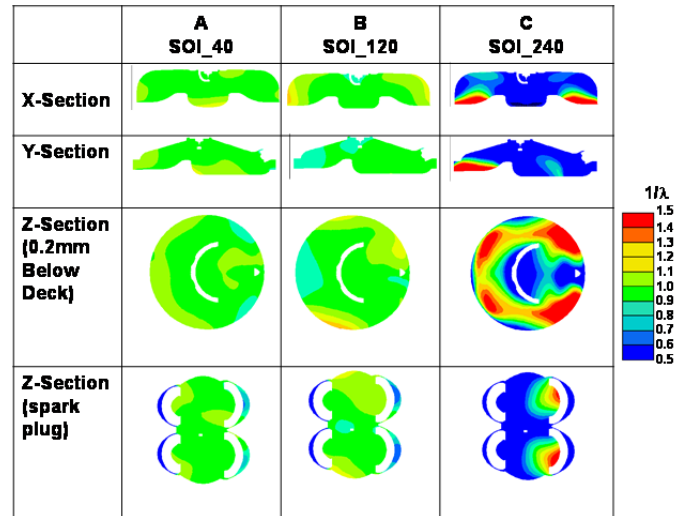

Figure 7. Fuel equivalence ratio (1/λ) in cylinder at 340° atdc-intake for selected SOI. The simulation was done without combustion. The charge non-uniformity, however, should be representative of the data in Fig. 5 where piston impingement takes place.

In set C, the injection was in the early to mid compression stroke. Some of the descriptions for set B apply but with two important exceptions: the time to combustion was shorter and, more importantly, the charge turbulence had decayed appreciably in the compression stroke (see Fig. 6). Both effects contributed to significant charge inhomogeneity (Fig. 7) leading to a high COV of NIMEP (Fig. 5). The higher PN emissions here were due to the presence of residual wall fuel films. Data on particle size spectra supporting that will be discussed in the next section.

In set A, injection was early in the intake stroke. A substantial amount of the fuel lands on the piston; see Table 2. More significantly, the fuel was injected into a charge of low density such that the fuel jet impinged on the piston at high momentum. Thus, a significant amount of the impinging fuel bounced off, collecting on the head and intake valve where the temperature is cooler. Because of the long lead time to combustion and because of the high piston surface temperature, it is expected that fuel on the piston almost completely evaporates. In addition, the high turbulence during the intake stroke renders a well-mixed charge (see Fig. 7) and stable combustion (see Fig. 5). The PN emissions, however, were high due to the residual liquid fuel on the head and intake valve surfaces where the temperature is closer to ECT and is substantially lower than the piston temperature. Data on the particle size spectra supporting that will be discussed in the next section. The PN decreases as SOI retards from 0° atdc-intake because (a) the piston is then further away so that the fuel jet momentum has diffused by the time it reaches the piston and the intensity of the fuel bounce is reduced; and (b) the piston is further away from the head so that the bounced fuel may not reach the head.

In set D, the injection was very close to spark discharge. Because of the limited mixing and evaporation time, the charge is highly inhomogeneous and there are significant liquid films on the piston. The piston bowl design, however, delivers a combustible mixture to the spark plug at the time of ignition such that a stable stratified combustion with reasonable COV of NIMEP was obtained; see Fig. 5. Because of the significant

liquid fuel films on the piston at flame arrival, however, the PN emissions were very high; see Fig. 4.

Particle size distribution

The particle size distributions also offer insight into the nature of particulate formation. The distributions for data set A (early injection) are shown in Fig. 8 together with the distribution of the first point at set B (at SOI=60° atdc-intake) for comparison. The former, with particles forming from liquid fuel films on the combustion chamber walls, shows higher particle numbers and larger particles which peak at 100 to 160 nm in diameter. The latter, with almost no wall fuel films at flame arrival and no significantly rich regions in the charge, shows very low particle numbers and much smaller particles, which peak at 30 nm. Thus the size spectra are different for particles formed with and without a significant presence of wall fuel films.
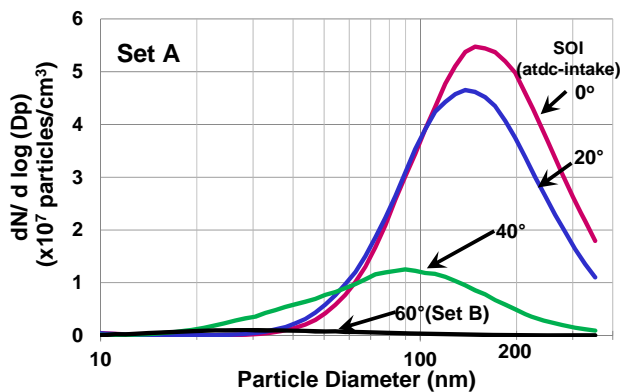

Figure 8. Particle size spectra of data set A plus the first point of data set B (at SOI=60° atdc-intake) in Fig. 4.

Representative particle size distributions for data set B in Fig. 4 are shown in Fig. 9. For this set, there were almost no wall fuel film when the flame arrived at the wall. The particles were formed in the locally rich regions of the charge. The particle numbers seen here are much lower than those in set A (the vertical axis scale has changed from that of Fig. 8). As the SOI changes, the particle numbers change, but the shape of the distribution remains the same. The peak is at approximately 20 to 30 nm in diameter.

It is observed that, for this data set, the PN values, which are low, are affected by the SOI timing. Therefore, the particles should be fuel related rather than originating from the lubrication oil.
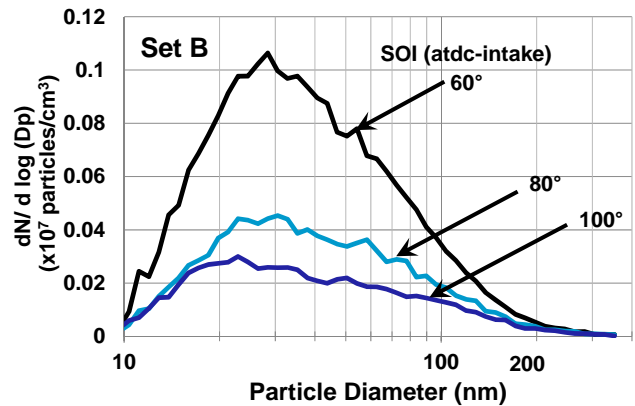

Figure 9. Representative particle size spectra for data set B in Fig. 4.

The particle size distributions for data sets C and D are shown in Fig. 10. In set C, the SOI was early in the compression stroke (up to 220° atdc-intake), resulting in adequate evaporation such that there were very little wall fuel films. Hence, the PN values were low and the particle sizes were small. As the injection was retarded, the time for evaporation and mixing decreased, so wall fuel films began to form and both the particle number and size increased.

For set D, injection was quite close to the spark timing. On the piston, there were significant wall fuel films which were the source of the particulate emissions. The particle numbers were high and larger particles (peaking at 180 nm in diameter) were measured. The similarity of the particle size spectrum in set D (Fig. 10) and in set A (Fig. 8) is noted. The similarity is indicative of the particulate formation from wall fuel films for both sets.
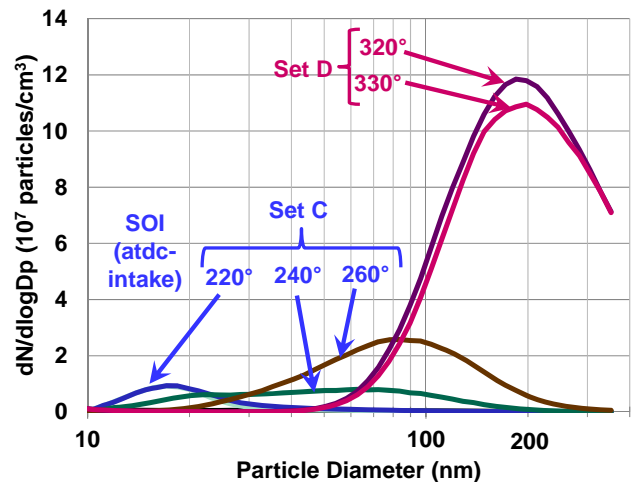

Fig. 10. Selected particle size spectra for data sets C and D in Fig. 4.

ECT effect

The PN emissions as a function of SOI at ECT of 20°C and 80°C are compared in Fig. 11. There is little difference in the emissions in the SOI range (60° to 240° atdc-intake) where PN emissions are low since, in this range, evaporation of the fuel films is already fast at the lower temperature. PN emissions are somewhat lower at the higher ECT when the SOI timing is retarded towards the mid stroke of compression (245° to 260°

atdc-intake). Emissions at late SOI (region D) are similar since, then, most of the impinging fuel lands on the piston. At the condition of the experiment, the piston temperature is sufficiently high (estimated to be 120C) such that evaporation is fast. Raising the ECT from 20 to 80C would change the piston temperature approximately from 120 to 180C. Although evaporation is facilitated by the higher piston temperature, it is not the rate limiting process for PM formation, which, for region D, is limited by mixing. Hence an insensitivity of PN to ECT has been observed..

Thus the major ECT effect is on the PN emissions with injection in the beginning of the intake stroke (region A). This observation is consistent with the explanation that PM formation here is from the fuel bouncing off of the piston onto the head. Then, the evaporation of the fuel film is sensitive to the head temperature which is close to the ECT. At 20C, PM formation from the wall fuel film would be limited by evaporation. Hence a change of ECT from 20C to 80C would substantially alter the evaporation rate and hence the PN emission.
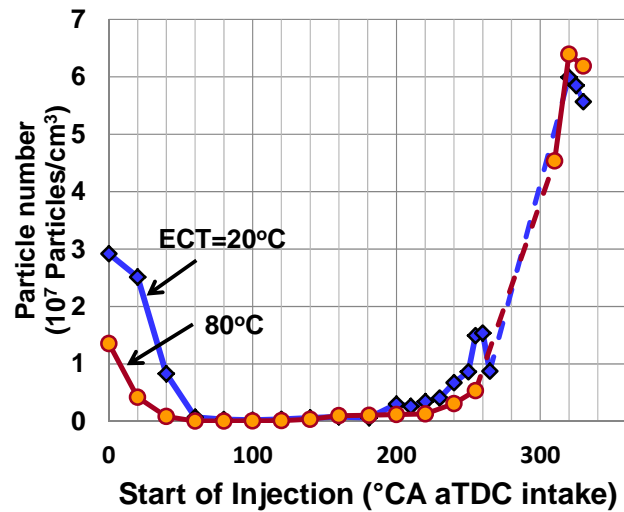

Figure 11. PN emissions at ECT=20° and 80° C. The engine does not fire in the data range denoted by the dashed lines.

Fuel effects

The base fuel (Haltermann HF0 437) is composed of 30.7% (by volume) aromatics, 0.5% olefins and 68.8% saturates. There are no oxygenates. GC analysis of the fuel sample indicated that there is no toluene. To investigate the effect of aromatics and ethanol on the PN emissions, the cold-fast-idle test (1200 rpm, 2 bar NIMEP, 20°C ECT and spark at -25° atdc-intake) was repeated with the base fuel blended with 15% and 30% (by volume) ethanol and again with 15% and 30% (by volume) toluene. The results are shown in Fig. 12. The emissions were moderately higher than those from the base fuel with the toluene blends, but were not substantially different with the ethanol blends.
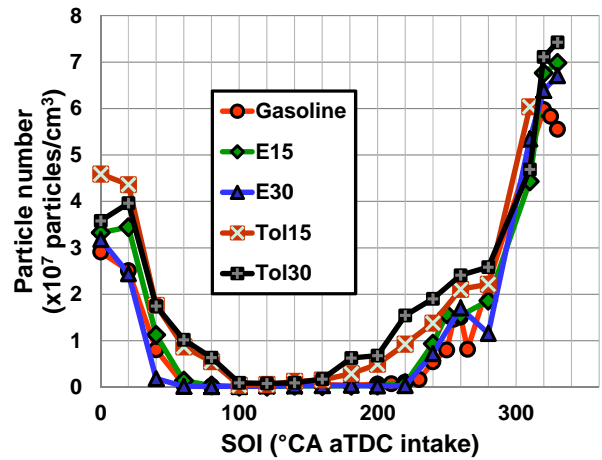

Figure 12. Comparison of PN emissions at cold-fast-idle for gasoline, gasoline/ ethanol blends and gasoline/ toluene blends.

Split injection

In cold start, spark retard is used to increase the enthalpy flow to the catalyst, thereby shortening the light-off time. To counteract the decreased engine stability associated with late spark timing, split injection is often employed. Part of the fuel is injected early in the cycle to create a well-mixed lean charge. Then, a second fuel pulse is introduced late in the compression process to supply a locally rich charge at the spark plug so that a robust combustion process is initiated.

To examine the PN emissions at cold-fast-idle with the above strategy, two injections with a fuel split of 70/30 by volume were employed. Based on the single injection result in the previous section, the first pulse was injected at 80° atdc-intake to create a well-mixed charge. The SOI of the second pulse was varied. The spark timing was significantly retarded, at 11° atdc-compression. The engine was again operated at 1200 rpm and 2 bar NIMEP.

The PN emissions as a function of the 2nd pulse SOI at combinations of intake air and coolant temperatures are shown in Fig. 13, together with the injection geometries. The piston positions are shown at the end of the injection; at that point, the fuel jet has reached the surface of the combustion chamber.

Unlike the single injection case, where misfire occurred when the SOI timing was in the range of 265° -320° atdc-intake, the combustion was stable for the whole range of the 2nd pulse SOI sweep, since a much smaller amount of fuel is being stratified.
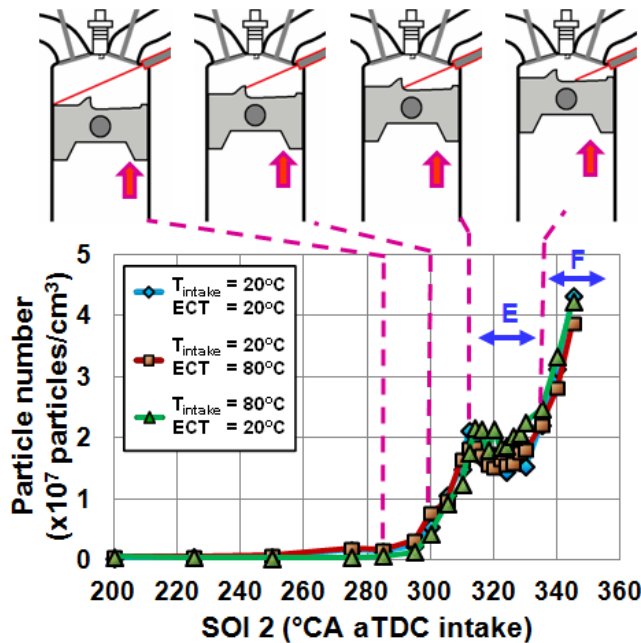
Figure 13. PN emissions with 70/30 split injection, as a function of 2nd pulse SOI for combinations of intake air temperatures and ECT.

Since the PN emissions here originate from the wall fuel film on the piston, and PM formation is limited by mixing rather than by the air or piston temperature the limiting factor for PM formation, the emissions values are not sensitive to the intake air and ECT temperatures.

Referring to Fig. 13, as a function of the 2nd pulse SOI, the PN emissions are seen to begin increasing when the fuel jet hits the piston and to increase rapidly when the fuel jet hits the piston bowl rim (see Fig. 1 for piston bowl geometry). However, in the region E (marked in Fig. 13), in which the impinging fuel was significantly collected in the bowl close to the piston bowl rim, the PN values decreased moderately before taking off again in region F.

The behavior of the PN emissions in region E may be explained by the intense mixing zone at the piston bowl rim that is created by the interaction of the shaped piston with the charge motion. The turbulent kinetic energy (TKE) from CFD calculations at 340° atdc-intake is shown in Fig 14. When the impinging fuel is collected in the region of high TKE, the fluid motion facilitates the evaporation and mixing processes, resulting in lower PN emissions. As the SOI is retarded, the impingement point on the piston moves away from the high TKE region, and PN emissions increase significantly.
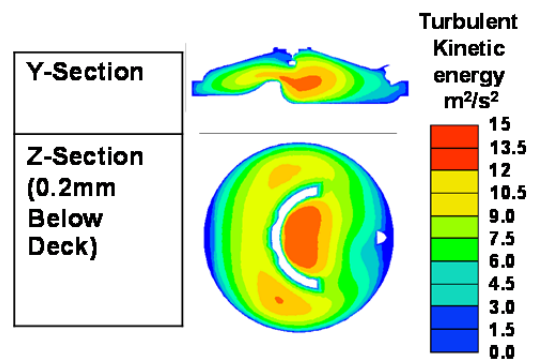

Figure 14. Turbulent kinetic energy in the piston bowl from CFD calculations at 340° atdc-intake.

A conceptual model for particulate formation

It is generally accepted that particulate emissions from SI engines are derived from the rich fuel air mixture derived from wall fuel films. Indeed, "pool fires" from these films have been reported [11-13]. A movie frame sequence showing the "pool fire" development from a liquid fuel film deliberately deposited on the piston [13, 15] is shown in Fig. 15. The propagating flame is shown in (a). The "pool fire" is first observed in (b), and further develops as the piston descends.
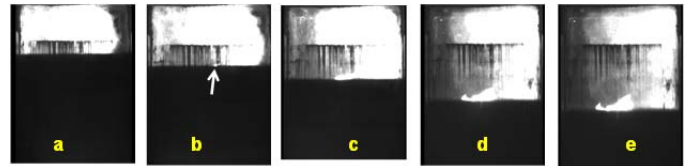

Figure 15. Frames of a movie obtained from a square piston engine showing a "pool fire" from a liquid fuel film on the piston [16]. The arrow in (b) marks the first appearance of the "pool fire."

An important realization is that the "pool fire" is completely submerged in the burned gas region. As such, there should be very little oxygen in the ambient gas since the combustion is stoichiometric. So, while the "pool fire" may have the appearance of a diffusion flame, it is not a diffusion flame since the ambient gas should not contain sufficient oxygen to support such a flame.

The above discussion leads to the following conceptual model describing the formation of particulate matter from wall fuel films. The following discussion refers to Figure 16.

1. Before flame arrival, the fuel evaporating from the film forms a vapor plume. The equivalence ratio within the plume varies from very rich at the surface of the film, to the value in the unburned gas at the outer edge. The unburned gas temperature is not sufficient to support soot formation in the plume [17].
2. When the flame arrives, the part of the plume within the flammability limit will burn. Some soot is formed in the rich flame. After flame passage, a rich fuel air mixture, demarcated by the flammability limit contour of the original plume, remains inside the hot burned gas; see Fig. 16 (b). The burned gas temperature is quite high. For reference,

cycle simulation results show that, at mid stroke of the expansion process, the value for the -25° atdc-compression spark case is 1500 K; that for the 11° atdc-compression spark case is 2000K. The heat conduction from the burned gases into the residual rich fuel air mixture is sufficient to initiate pyrolysis and particulate formation.

3. At the boundary between the hot burned gases and the residual rich mixture, heat conduction from the burned gases and the heat release from the pyrolysis process sustain a soot formation region in the rich mixture. Radiation from the particles in this region appears as the "pool fire," which develops further as more fuel vapor evaporates from the fuel film. The size of the "pool fire" grows by diffusion and by expansion due to the descending piston.
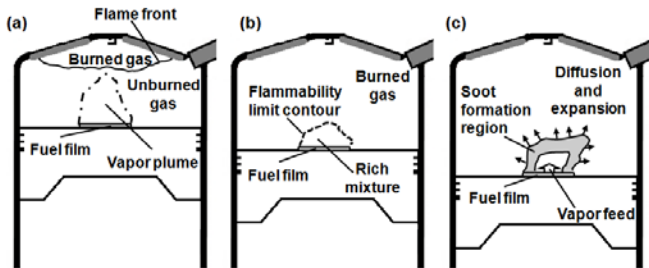

Figure 16. A conceptual model of the soot formation process from residual fuel films.

In summary, the "pool fire" that is often observed in cold-start engine combustion is really not a fire, in the sense that there is no diffusion flame. This absence is because there is little ambient oxygen in the surrounding burned gases to support such a flame. The visible radiation is from the hot soot particles formed in the pyrolysis process in the residual fuel rich region that is beyond the flammability limit. The pyrolysis is sustained by heat conduction from the ambient hot burned gases and by the heat released in the pyrolysis process.

To further confirm that the particulate formation is not due to a diffusion flame, the PN emissions were measured in an equivalence ratio sweep. In this set of experiments, the amount of liquid fuel was fixed so that the engine was running at a lean condition. Then, propane was injected in the intake port to increase the fuel equivalence ratio (Φ). Thus, the liquid fuel delivery process and the wall fuel film formation processes remained the same throughout the sweep.

Three sweeps were conducted:

a. With a single injection at approximately the mid stroke of the intake process (SOI = 100° atdc-intake). In this case, as shown previously (see Fig. 4), there should be a very low wall film mass and low PN emissions.
b. With a single injection early in the intake process (SOI = 40° atdc-intake). In this case there are significant PN emissions due to the wall films formed from fuel rebounding off of the piston (see Fig. 4 and the associated discussion).
c. With split injection (70/30 by volume) with the first injection at 80° and second injection at 320° atdc-intake. In this

case, significant PN emissions are formed due to the collection of liquid fuel in the piston bowl.

The results of these experiments are shown in Fig. 17. It is noted that as the charge equivalence ratio goes from rich to lean, there is no significant jump in the PN values. If the particles were formed by a diffusion flame using the residual oxygen in the burned gases, there should have been a substantial difference observed since the flame would be very different given the significant oxygen concentrations in the burned gases when the charge is lean.
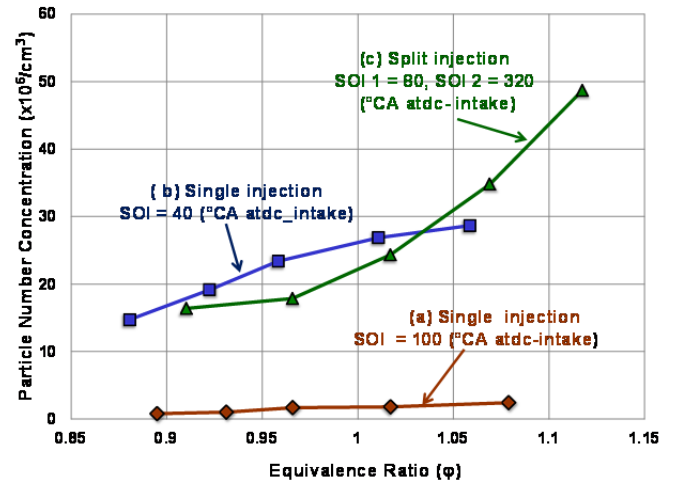

Figure 17. PN emissions as function of fuel equivalence ratio of the charge. For each curve, only liquid fuel is used for the data point at the lowest Φ. Then, Φ is increased by augmenting this fuel with port-fuel-injection of propane.

Summary/Conclusions

The nature of particulate formation in a production direct-injection spark-ignition engine was studied under cold-fast-idle conditions (1200 rpm, 2 bar NIMEP, 20° C ECT). The following conclusions were drawn:

1. The particulate emissions originate from the wall fuel films produced by the fuel jet. The presence of these films and the resulting PN emissions depend on the geometry of the spray with respect to the combustion chamber and the charge motion which affects the film evaporation and vapor/ air mixing processes.
2. When injection is early in the intake stroke, there are high PN emissions due to the wall films formed on the cylinder head from the fuel splashing off of the piston crown.
3. Injection in the mid to late intake stroke produces very low PN emissions. The large footprint of the wall-impinging fuel and the high turbulence produced by the charge induction facilitate evaporation and mixing, thus suppressing wall film formation.
4. PN emissions increase when injection takes place in the compression stroke, and increase drastically when the fuel jet hits the piston. The increase is due to the substantially shorter time for evaporation and mixing before the flame arrival at the fuel film on the piston.
5. A conceptual model was developed to describe the process of particulate formation from wall fuel films. The

formation is from pyrolysis in the rich residual fuel/air mixture after flame passage. The process is sustained by heat transfer from the hot burned gases and by the heat release from the pyrolysis reactions.

References

1. Bandel, W., Fraidl, G., Kapus, P., Sikinger, H. et al., "The Turbocharged GDI Engine: Boosted Synergies for High Fuel Economy Plus Ultra-low Emission," SAE Technical Paper 2006-01-1266, 2006, doi:10.4271/2006-01-1266.
2. Woldring, D., Landenfeld, T., and Christie, M., "DI Boost: Application of a High Performance Gasoline Direct Injection Concept," SAE Technical Paper 2007-01-1410, 2007, doi:10.4271/2007-01-1410.
3. Davis, R., Mandrusiak, G., and Landenfeld, T., "Development of the Combustion System for General Motors' 3.6L DOHC 4V V6 Engine with Direct Injection," SAE Int. J. Engines 1(1):85-100, 2009, doi:10.4271/2008-01-0132.
4. McNeil, S., Adamovicz, P., and Lieder, F., "Bosch Motronic MED9.6.1 EMS Applied on a 3.6L DOHC 4V V6 Direct Injection Engine," SAE Technical Paper 2008-01-0133, 2008, doi:10.4271/2008-01-0133.
5. Whitaker, P., Kapus, P., Ogris, M., and Hollerer, P., "Measures to Reduce Particulate Emissions from Gasoline DI engines," SAE Int. J. Engines 4(1):1498-1512, 2011, doi:10.4271/2011-01-1219.
6. Sabathil, D., Koenigstein, A., Schaffner, P., Fritzsche, J. et al., "The Influence of DISI Engine Operating Parameters on Particle Number Emissions," SAE Technical Paper 2011-01-0143, 2011, doi:10.4271/2011-01-0143.
7. Piock, W., Hoffmann, G., Berndorfer, A., Salemi, P. et al., "Strategies Towards Meeting Future Particulate Matter Emission Requirements in Homogeneous Gasoline Direct Injection Engines," SAE Int. J. Engines 4(1):1455-1468, 2011, doi:10.4271/2011-01-1212.
8. Peckham, M., Finch, A., Campbell, B., Price, P. et al., "Study of Particle Number Emissions from a Turbocharged Gasoline Direct Injection (GDI) Engine Including Data from a Fast-Response Particle Size Spectrometer," SAE Technical Paper 2011-01-1224, 2011, doi:10.4271/2011-01-1224.
9. Commission Regulation (EU) No 459/2012.
10. Shin, Y., Cheng, W., and Heywood, J., "Liquid Gasoline Behavior in the Engine Cylinder of a SI Engine," SAE Technical Paper 941872, 1994, doi:10.4271/941872.
11. Witze, P. and Green, R., "LIF and Flame-Emission Imaging of Liquid Fuel Films and Pool Fires in an SI Engine During a Simulated Cold Start," SAE Technical Paper 970866, 1997, doi:10.4271/970866.
12. Stevens, E. and Steeper, R., "Piston Wetting in an Optical DISI Engine: Fuel Films, Pool Fires, and Soot Generation," SAE Technical Paper 2001-01-1203, 2001, doi:10.4271/2001-01-1203.
13. Costanzo, V. and Heywood, J., "Effect of In-Cylinder Liquid Fuel Films on Engine-Out Unburned Hydrocarbon Emissions for an SI Engine," SAE Technical Paper 2012-01-1712, 2012, doi:10.4271/2012-01-1712.
14. Cheng, W.K., Summers, T., Collings, N.,"The Fast-Response Flame Ionization Detector," Prog. in Energy and Comb. Sc., 24, 89-124, 1998.
15. Kaplan, J., "Modleing the Spark Ignition Engine Warm-Up Process to Predict Component Tempertures," MS thesis, Department of Mech. Eng., MIT, 1990.
16. Movie frames in Fig. 15 are derived from Vince Constanzo's thesis work: "Effect of In-cylinder Liquid Fuel Films on Engine-Out Unburned Hydrocarbon Emissions for SI Engines," PhD thesis, Dept. of Mech. Eng., MIT, Feb., 2011.
17. Akihama, K., Takatori, Y., Inagaki, K., Sasaki, S. et al., "Mechanism of the Smokeless Rich Diesel Combustion by Reducing Temperature," SAE Technical Paper 2001-01-0655, 2001, doi:10.4271/2001-01-0655.

Contact Information

Justin Ketterer, justin.ketterer@gm.com

Wai Cheng, wkcheng@mit.edu

Acknowledgments

.

Definitions/Abbreviations

atdc	After top-dead-
CFD	Computational fluid dynamic
DI	Direct injection
ECT	Engine coolant temperature
NIMEP	Net indicated mean effective pressure
PM	Particulate matter
PN	Particulate number; totaled from 23 to 350 nm
RON	Research Octane number
SI	Spark ignition
SOI	Start of injection
Φ	Fuel equivalence ratio
λ	Air equivalence ratio